

Article

On the Equivalence of the Switched Inductor and the Tapped Inductor Converters and its Application to Small Signal Modelling

Jia Yao ^{1,*} , Kewei Li ¹, Kaisheng Zheng ¹ and Alexander Abramovitz ²

¹ Department of Electrical Engineering, School of Automation, Nanjing University of Science and Technology, Nanjing 210094, China; likewei@njust.edu.cn (K.L.); zks471945188@gmail.com (K.Z.)

² Faculty of Engineering, Holon Institute of Technology, Holon 5810201, Israel; alabr@hotmail.com

* Correspondence: yaojia@njust.edu.cn; Tel.: +86-1360-140-1811

Received: 7 November 2019; Accepted: 16 December 2019; Published: 17 December 2019



Abstract: Switched inductor (SI) converters are popular in applications requiring a steeper conversion ratio. However, these converters operate a twin inductor switching cell, which complicates the small-signal modeling. This paper proposes an expeditious small-signal analysis method to model the SI converters. The offered modeling approach is hinged on the analogy existing between the SI converters and certain Tapped Inductor (TI) converters. It is suggested here that by virtue of the analogy of the SI converters and TI converters the small-signal model of the SI converter is identical to that of its ideal TI counterpart. Hence, the recently developed Tapped Inductor Switcher (TIS) methodology can be applied to the modeling of the SI converters as well. As an example, the small-signal model of the Switched Inductor Buck converter is obtained. Theoretical analysis was confirmed by simulation and experimental results. In addition, several other SI converters and their TI counterparts are identified.

Keywords: high order dc/dc converter; unified modeling cell; switched inductor; tapped inductor

1. Introduction

Renewable energy applications, such as solar and fuel cell-based energy generation systems produce low DC voltage that has to be stepped up significantly to match the grid level. To meet the challenge, a number of high gain converters were developed and reported in recent literature. Tapped Inductor (TI) converters are a well-known class of converters and are quite popular for renewable energy applications that use a coupled magnetic device with several but, in most cases, just two windings [1–3] to attain higher gain. As compared to their uncoupled counterparts TI converters can attain wider conversion ratio by a proper choice of the turn ratio and winding polarity. Yet, this desirable feature comes at a price of pulsating currents and higher voltage stress. The switch voltage stress in TI converters is further aggravated by the leakage inductance discharge. To lower the voltage spike across the semiconductors as well as increase the efficiency of the power stage, the clamp and snubber circuits have to be employed to capture the leakage energy [3–5]. Snubbers, however, usually have a limited performance envelope, affect the converter's conversion ratio, and complicate the converter's design.

An alternative solution to attaining a wider conversion ratio is using the switched inductor (SI) and switched capacitor (SC) cells [6–8]. SI converters can achieve moderately wider conversion ratio and may have an advantage over the TI converters with similar specifications. The key benefit of the SI cells is that they are free from problems associated with the leakage inductance. Therefore, SI converters exhibit lower voltage stress and may need no snubbers [9–11]. The increasing popularity

of the SI converters can also be attributed to their simplicity, robustness, and modest cost. For these reasons, SI converters became particularly popular in the field of alternative and renewable energy power generation, such as PV applications [12–15].

As shown in Figure 1, switched inductor cells consist of two inductors and multiple diodes. The large component count and switching action may bring complications to analysis and modeling. State space averaging (SSA) [16] was one of the most popular modeling techniques for switching converters, which can also be employed to analyze SI converters [15]. However, for more complicated topologies, such as multiple SI cells [17], extended SI cells with switched capacitor [12], hybrid SI cells [18], complicated and tedious formula derivations were required when using the SSA method. An attempt to derive the equivalent circuit model of SI cell has been reported in [19], however it only discussed the circuit model to the proposed topology. A unified equivalent circuit model of a hybrid type SI cell was proposed in [20]. The method may cover a wide range of converters but cannot be used for traditional SI cell converters.

Recently an equivalence in between SI Boost and TI Boost converters was suggested [21]. As reported, under equivalence conditions the ideal SI Boost and its ideal equivalent TI Boost converter are functionally identical as far as their terminal voltages and currents as well as conversion ratio are concerned. The equivalence holds in both continuous and discontinuous modes. Moreover, the equivalent converters have identical frequency responses. This implies that their dynamic models are also identical.

While in [21] a step-up SI cell was examined, in this paper, with the aim to extend the method further, the step-down SI cell is investigated. Here, the equivalence existing between a number of additional SI converters and their candidate TI equivalent counterparts is revealed. The paper also offers small signal modeling approach of SI converters that can be accomplished in two easy steps. First, the problem SI converter is examined, and its equivalent TI topology is found. Then, taking the advantage of the equivalence feature, the Tapped Inductor Switcher (TIS) model [22] is applied to the equivalent TI topology. This yields the desired dynamic model of the SI converter.

This paper is organized as follows. Firstly, three basic types of SI cells are reviewed. Then the equivalence conditions of SI Buck, SI Buck-Boost, and SI Boost with their Tapped Inductor counterpart are presented. According to the proposed equivalence methodology, high order hybrid converters with SI cells and their equivalent tapped-inductor converters are discussed in Section 6. Based on the equivalence between SI converters and TI converters, the unified tapped inductor switcher modeling method (TIS) is studied in Section 7. As an application example, the small-signal model of the SI Buck converters is derived. The analysis results are confirmed by simulation and experiment.

2. Brief Review of the Switched Inductor Cells

The SI cells, illustrated in Figure 1, are comprised of a pair of equal valued inductors and a passive (diode only) switching network [6]. Such SI cells can be used as building blocks of various step-up and step-down dc-dc converters. An SI variant converter can be derived from its traditional counterpart by replacing the regular inductor by the switched inductor cell. The SI cells in Figure 1a,b can be used in step-down topologies, whereas SI cell in Figure 1c can provide step-up action.

The SI step-up cell in Figure 1c has just one pair of terminals. Hence, the SI step-up cell can point-by-point replace an ordinary inductor and readily modify a step-up converter. However, the SI step-down cells in Figure 1a,b are two-port networks that have to be installed on both the feed and return lines. The latter, however, keeps the output floating.

Moreover, taking a closer look at Figure 1a and unfolding the twisted wiring reveals that the circuit can be redrawn similarly to an H bridge as shown in Figure 2. The same drill can be repeated in Figure 1b, which leads to the same Figure 2. Here it becomes obvious that the circuits in Figure 1a,b differ only in the designation of the output (load) terminals. That is, except for the polarity of the output voltage, both cells are identical. Since the polarity of the output voltage is merely a matter of

convention, such a minor difference is immaterial. Therefore, in the following, only the SI step-down cell in Figure 2 is considered.

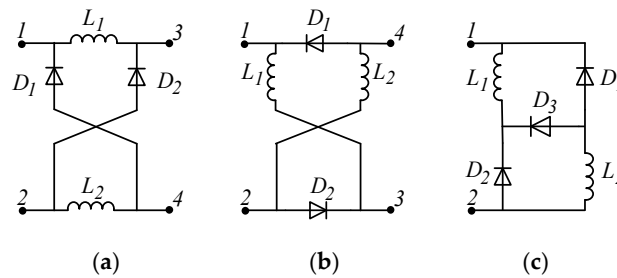


Figure 1. The Switched Inductors cells [6]: (a) non-inverting step-down cell; (b) the inverting step-down cell; (c) the step-up cell.

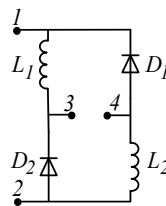


Figure 2. Generic step-down Switched Inductor cell.

3. Equivalence of the SI Buck and TI Buck Converters

3.1. Review of the SI Buck Converter

The Switched Inductor Buck (SIBk) converter can be derived off the traditional Buck by imbedding the SI cells as suggested in Figure 3a. The resulting SIBk is a single switch, simple, and rugged topology. As already mentioned, SI Buck can achieve a steeper conversion ratio than the traditional Buck converter and operate in a wider duty cycle range.

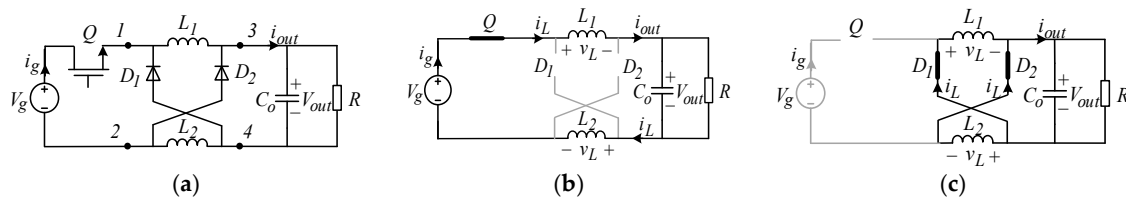


Figure 3. Ideal Non-Inverting SI Buck converter: (a) topology; (b) on-state equivalent circuit; (c) off-state equivalent circuit.

In the following it is assumed that SI Buck in Figure 3a is comprised of ideal components, i.e., the switches have zero switch-on resistance and no forward voltage drop, and the inductors have zero resistance. It is also assumed that the converter operates in CCM (Current Continuous Mode), so that its switching cycle is comprised of only two intervals: the “on” interval and the “off” interval.

When the active switch in the SI Buck converter is on, a positive voltage, V_g , is applied to the cell’s input terminals 1 and 2 (see Figure 3b); the diodes are switched off forcing the inductors to assume series configuration and charge up. Since SI cell is comprised of equally sized inductors, $L_1 = L_2 = L$, the equivalent “on” state inductance of the SI Buck (see Figure 3b) is

$$L_{on} = L_1 + L_2 = 2L \quad (1)$$

When the active switch is turned off, the diodes turn on to freewheel the inductors’ currents as shown in Figure 3c with both inductors discharging in parallel to the output. Hence, it is evident (see Figure 3c) that the equivalent “off state” inductance of the SI Buck is

$$L_{off} = \frac{L_1 L_2}{L_1 + L_2} = \frac{1}{2} L \quad (2)$$

3.2. Review of the TI Buck Converter

The topology shown in Figure 4a can be classified as diode-to-tap Tapped Inductor Buck converter with cumulative windings. Henceforth, the topology in Figure 4a is referred to as the TI Buck (TIBk) converter.

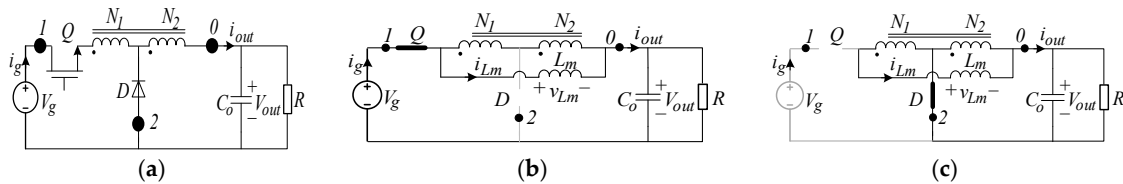


Figure 4. Ideal TIBk converter: (a) topology; (b) on-state equivalent circuit; (c) off-state equivalent circuit.

In the following it is assumed that the candidate TIBk converter is ideal (i.e., lossless switches and the ideal tapped inductor with neither leakage nor resistance).

During the “on” interval (see Figure 4b), the tapped inductor charges through a series cumulative connection of both the primary, N_1 , and secondary, N_2 , windings having the equivalent inductance of

$$L'_{on} = L_m \quad (3)$$

Here, the magnetizing inductance, L_m , is defined as the combined inductance of both N_1 and N_2 windings (see Figure 4).

During the “off” interval (see Figure 4c), the active switch is turned off while the diode freewheels the magnetizing current to the output through the N_1 winding. Thus, through the autotransformer action of the tapped inductor, the equivalent inductance is

$$L'_{off} = L_{N2} = L_m \left(\frac{n}{n+1} \right)^2 \quad (4)$$

Here $n = N_2/N_1$ is the TI's turn ratio.

3.3. Derivation of the SIBk and TIBk Equivalence Conditions

The hypothesis proposed herein is that if the parameters of the TIBk converter are adjusted to fulfill the following constraints: $L'_{on} = L_{on}$ and $L'_{off} = L_{off}$, the resulting TIBk converter can precisely imitate the function of SIBk converter and, thus, can be considered as a functional equivalent (with the exception of different voltage stress across the switches).

Therefore, the necessary equivalence conditions between SIBk and TIBk converters can be obtained equating Equations (1) to (3) and (2) to (4). This yields the following:

$$L_m = 2L \quad (5)$$

$$n = 1 \quad (6)$$

In other words, the tapped inductor of the equivalent TIBk converter should have an equal turn winding arrangement, which inductances relate to its SI counterpart according to:

$$L_{N1} = L_{N2} = L_m \left(\frac{n}{n+1} \right)^2 = L/2 \quad (7)$$

Moreover, since SIBk inductances are equally valued, compared with Figure 3b,c and Figure 4b,c, it is evident that, under the equivalence conditions, the TIBk's magnetizing inductance voltage and current are related to SIBk's inductors' voltage and current by

$$v_{Lm} = 2v_L \quad (8)$$

$$i_{Lm} = i_L \quad (9)$$

3.4. Comparison of the SIBk and TIBk Simulation Results

To verify the hypothesis above, benchmark SIBk and its equivalent TIBk were simulated in time domain by PSIM 9.1.4. Both converters were operated with identical duty cycle, D , and had identical filter capacitor C_o ; identical load R ; as well as identical input voltage, V_g . Since this paper aims to study small-signal behavior of SI converters, which have no leakage, the leakage inductance in its TI counterpart is not considered. For this reason, the tapped inductor was simulated by the ideal transformer model in parallel with magnetizing inductance.

The parameters of the benchmark SIBk converter were $L_1 = L_2 = 200 \mu\text{H}$ at CCM and $2 \mu\text{H}$ at discontinuous conduction mode (DCM), $V_g = 24 \text{ V}$, $D = 0.5$, $R = 10 \text{ Ohm}$, $C_o = 47 \mu\text{F}$, $f_s = 50 \text{ kHz}$. The equivalent TIBk converter parameters calculated by Equations (5) and (6) were $n = 1$ and $L_m = 400 \mu\text{H}$ for CCM and $4 \mu\text{H}$ for DCM. Zero leakage inductance was assumed.

Comparison of key simulated waveforms of both converters in the CCM mode is shown in Figure 5a, whereas the DCM waveforms comparison is presented in Figure 5b. In both cases the simulated responses of both SIBk and its equivalent TIBk converters were found to be precisely identical.

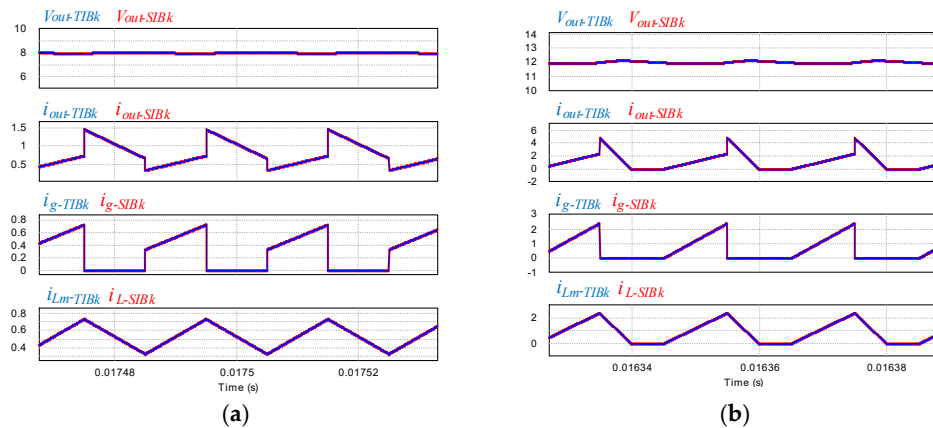


Figure 5. Comparison of time domain waveforms of an ideal Switched Inductor Buck (SIBk) vs. the equivalent Tapped Inductor Buck (TIBk) converters: (a) CCM; (b) discontinuous conduction mode (DCM). Top trace: output voltage, V_o ; second trace: the output current, i_{out} ; third trace: the input terminal current, i_g ; bottom trace: the inductor current, i_L .

The frequency response of the ideal SIBk and that of its equivalent ideal TIBk converters was compared and is plotted in Figure 6. As expected, the results are precisely matched. Thus, the notion of the equivalence of SIBk and TIBk converters is confirmed.

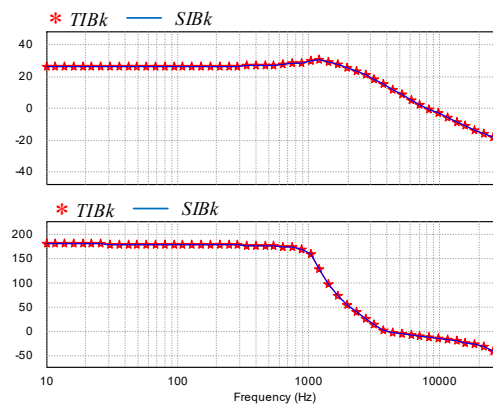


Figure 6. Comparison of simulated small-signal duty-cycle to output voltage frequency response of the benchmark SIBk converter (solid blue) vs. the equivalent TIBk converter (star, red). Both converters operate in CCM.

4. Equivalence of The SI Buck-Boost and TI Buck-Boost Converters

4.1. Preliminary Considerations and Basic Assumptions

Both the step-down cells in Figure 1a,b seem incompatible with the Buck-Boost converter. However, by imbedding the step-up SI cell in Figure 1c into the traditional Buck-Boost topology, the Switched Inductor Buck-Boost (SIBB) converter can be derived as shown in Figure 7a [6].

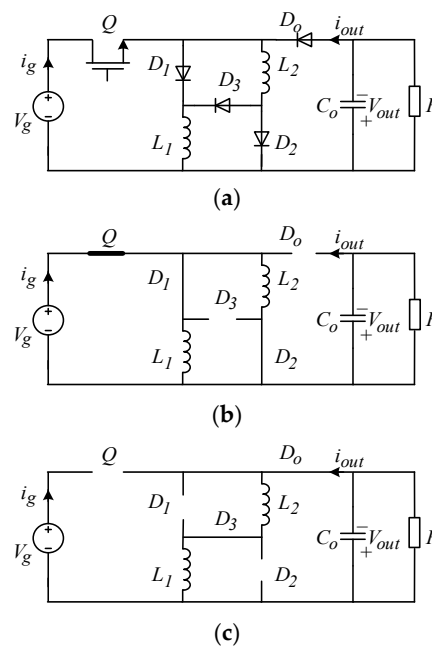


Figure 7. Ideal Switched Inductor Buck-Boost (SIBB) converter: (a) topology; (b) on-state equivalent circuit; (c) off-state equivalent circuit.

The same as above, it is assumed here that SIBB is made of ideal and lossless components, operates in CCM, and its inductors are identical, that is $L_1 = L_2 = L$.

4.2. Review of the SIBB Converter

Examining the SIBBs on state equivalent circuit in Figure 7b reveals that the equivalent on state inductance seen between the input and the switch terminals is

$$L_{on} = \frac{L_1 L_2}{L_1 + L_2} = \frac{1}{2} L \quad (10)$$

Whereas during the off interval, the off inductance of the SI Buck-Boost seen between the input and output terminals (see Figure 1c) is

$$L_{off} = L_1 + L_2 = 2L \quad (11)$$

4.3. Review of the TIBB Converter

The candidate equivalent Tapped-Inductor Buck-Boost topology (TIBB) is shown in Figure 8a and can be classified as switch-to-tap TI converter with cumulative windings.

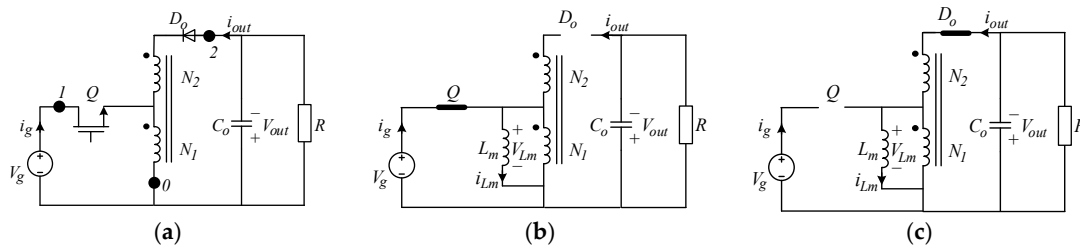


Figure 8. Ideal Tapped-Inductor Buck-Boost (TIBB) converter: (a) topology; (b) on-state equivalent circuit; (c) off-state equivalent circuit.

In the following, an ideal TIBB (i.e., lossless switches and the ideal tapped inductor with negligible leakage) which operates in CCM is considered.

During the on interval (see Figure 8b) the active switch energizes only the N_1 winding. Thus, equivalent inductance seen between the input and the switch terminals (0, 1) is

$$L'_{on} = L_m, \quad (12)$$

where the magnetizing inductance, L_m , is referred to as the N_1 winding as shown in Figure 8b.

During the “off” interval (see Figure 8c), the active switch is turned off while the diode freewheels the magnetizing current to the output through both the primary N_1 , and the secondary N_2 windings. Thus, through the autotransformer action of the tapped inductor, the equivalent inductance seen between the terminals (0, 2) is

$$L'_{off} = (1 + n)^2 L_m. \quad (13)$$

Here, $n = N_2/N_1$ is the turn ratio.

4.4. Derivation of the SIBB and TIBB Equivalence Conditions

Equivalence conditions between SIBB and TIBB converters can be derived equating Equations (12) to (10) and (13) to (11) yielding

$$L_m = \frac{1}{2} L, \quad (14)$$

$$n = 1. \quad (15)$$

Hence, regardless of the definition of the magnetizing inductance, the ratio of self-inductances of the tapped inductor of the equivalent TIBB can be derived by Equation (14) which is same as described by Equation (7).

4.5. Comparison of the SI Buck-Boost and TI Buck-Boost Simulation Results

A benchmark SIBB and its equivalent TIBB were simulated in time domain. Both converters were operated with identical duty cycle, D , and had identical filter capacitor C_o ; identical load R ; as well as identical input voltage, V_g .

The parameters of the benchmark SIBB converter were $L_1 = L_2 = 200 \mu\text{H}$ at CCM and $2 \mu\text{H}$ at DCM, $V_g = 24 \text{ V}$, $D = 0.5$, $R = 10 \Omega$, $C_o = 47 \mu\text{F}$, $f_s = 50 \text{ kHz}$. The equivalent TIBB converter parameters calculated by Equations (14) and (15) were $n = 1$ and $L_m = 100 \mu\text{H}$ at CCM and $1 \mu\text{H}$ at DCM. Zero leakage inductance was assumed.

Comparison of key simulated time domain waveforms of both converters in the CCM mode is shown in Figure 9a, whereas the discontinuous conduction mode (DCM) waveforms comparison is presented in Figure 9b. In both cases the simulated responses of both SIBB and its equivalent TIBB converters were found to be precisely identical.

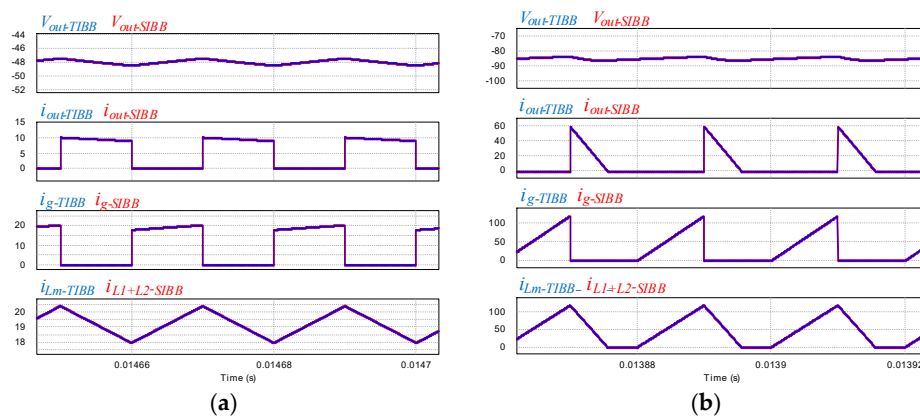


Figure 9. Comparison of time domain waveforms of an ideal SIBB vs. the equivalent TIBB converters: (a) CCM; (b) DCM. Top trace: output voltage, V_o ; second trace: the output current, i_o ; third trace: the input terminal current, i_g ; bottom trace: the inductor current, i_L .

The small signal duty-cycle to output frequency response of the ideal SIBB and that of its equivalent ideal TI Buck-Boost converters was also compared and is plotted in Figure 10. The results are precisely matched. Thus, the simulation results further support the notion of the equivalence of SIBB and TIBB converters.

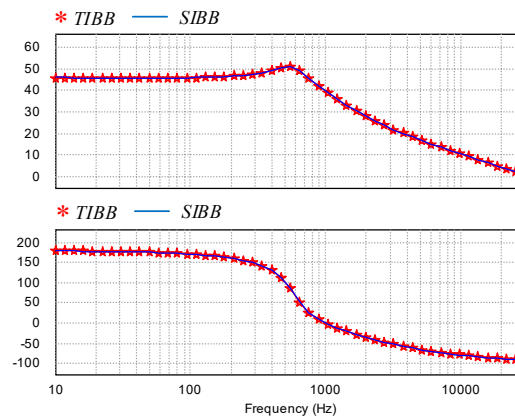


Figure 10. Comparison of simulated small-signal duty-cycle to output voltage frequency response of the benchmark SIBB converter (solid blue) vs. the equivalent TIBB converter (star, red). Both converters operate in CCM.

5. Equivalence of the SI Boost and TI Boost Converters

The SI Boost (SIB) converter shown in Figure 11 and its equivalent TI Boost (TIB) converter in Figure 12 were analyzed earlier [21]. Here, for completeness of this text, only the equivalence conditions between SIB and TIB are briefly mentioned.

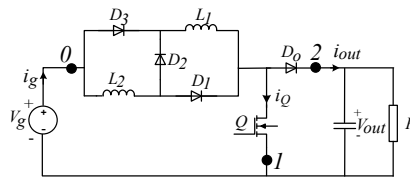


Figure 11. Ideal SIB (Switched Inductor Boost) converter topology.

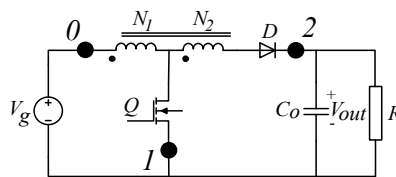


Figure 12. Ideal TIB (Tapped Inductor Boost) converter topology.

The SIB in Figure 11 applies the step-up SI cell, the same as SIBB in Figure 7. Hence, applying the same considerations as described in the previous section, the equivalence conditions of the SIB and TIB are found identical to Equations (14) and (15), where the magnetizing inductance L_m is referred to the N_1 winding of TI in Figure 12. The basic hybrid converters with switched-inductor cells and their equivalent tapped-inductor counterparts were presented in Table 1.

Table 1. Basic hybrid converters with switched-inductor cells and their equivalent tapped-inductor counterparts.

Type	Buck	Boost	Buck-Boost
SI			
Eq. TI			
Param. ratio	$L_1 = L_2 = L; L_{N1} = L_{N2} = L/2; N_1 = N_2$		

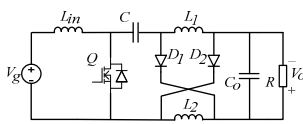
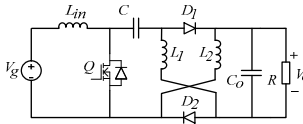
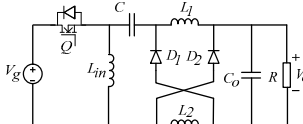
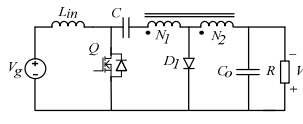
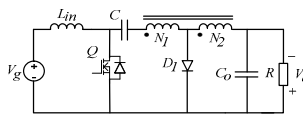
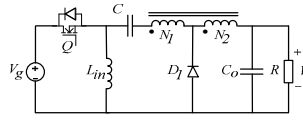
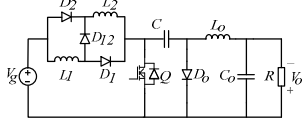
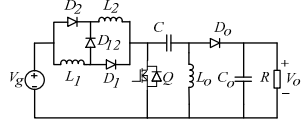
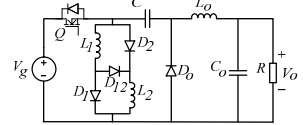
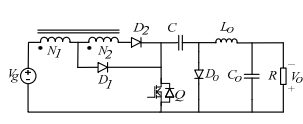
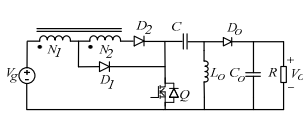
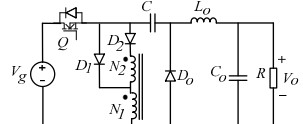
6. High Order SI Converters and Their Equivalent TI Counterparts

The SI step-up and SI step-down cells in Figure 1 can be applied to modify many other converters as well [23–25]. The SI variants of Cuk, Sepic, and Zeta topologies were also derived in [26]. Yet, constructing the TI equivalent counterparts of these topologies requires deeper consideration.

Firstly, consider the step-down converters. According to [6], the SI Cuk in Table 2 (a) applies the SI cell in Figure 1a, whereas the SI SEPIC in Table 2 (b) makes use of SI cell in Figure 1b. However, as mentioned, both cells are identical (except for the polarity of the output voltage) therefore, both circuits in Table 2 (a) and (b) can be considered identical. For this reason, both converters have the

same TI equivalent counterpart as illustrated in Table 2 (d) and (e). The step-down SI Cuk and its TI counterpart are shown in Table 2 (e) and (f).

Table 2. High order hybrid converters with switched-inductor cells and their equivalent tapped-inductor counterparts.

Type	Cuk	SEPIC	Zeta
Step-Down	 <p>(a)</p>	 <p>(b)</p>	 <p>(c)</p>
	 <p>(d)</p>	 <p>(e)</p>	 <p>(f)</p>
Step-Up	 <p>(g)</p>	 <p>(h)</p>	 <p>(i)</p>
	 <p>(j)</p>	 <p>(k)</p>	 <p>(l)</p>
Param. ratio	$L_1 = L_2 = L; L_{N1} = L_{N2} = L/2; N_1 = N_2$		

Next, refer to the step-up SI Cuk, Sepic, and Zeta converters in Table 2. These topologies comprise of a series capacitor in between the active switch and the output diode (the passive switch). Thus, in these cases, the simple tap-to-switch TI arrangement used to construct the equivalent TI Cuk and the equivalent TI Sepic converters (see Table 2 (d) and (e)) cannot be applied. Using two active switches makes it possible but such a scheme undermines the idea of equivalence. Therefore, in order for the equivalent TI converter to retain the single switch feature, a special “two-terminal” tapped inductor configuration can be applied to substitute the step-up SI cell, as shown in Table 2 (j), (k), and (l).

The derived above rules of equivalence Equations (5)–(7), (14) and (15)) also apply to the high order step-up and step-down converters. A simulation study was launched to compare the SI topologies to their proposed TI equivalent counterparts in Table 2. The simulated waveforms are presented in Appendix A which confirm the theoretical predictions.

7. Application to Small Signal Modelling of Switch Inductor Converters

Switched inductor cells consist of two inductors and multiple diodes. The switching action brings complications to modeling. Due to the equivalence of switched inductor and tapped inductor converters, the dynamic and steady state model of the SI converters can be obtained by borrowing and adapting the models of the equivalent TI counterpart. Earlier, an approach to modelling of tapped inductor converters was suggested in [22]. The proposed Tapped Inductor Switcher with Switched Flow Graph (TIS-SFG) method relies on substituting the switching part of the converter by a prefabricated equivalent subgraph. Such modeling approach proved expeditious and well-suited to tapped inductor converters. For these reasons TIS-SFG is also a viable candidate to modeling of SI converters.

While in [21] a step-up SI cell was examined and modeled by the proposed method, here, with the aim to extend the method further, the step-down SI cell is studied in detail. As an application example, in the following, small-signal model of the SI Buck is derived and verified by simulation and experiment.

7.1. Brief Review of TIS-SFG Modeling Approach

The TIS-SFG method relies on point-by-point substitution of the tapped inductor switching block of the converter (see Figure 13a) by its equivalent sub-graph shown in Figure 13b. Here, $K(D)$ represents the active switch function and placed at terminal 1, while $K'(D')$ stands for the passive (or complementary) switch at terminal 2. The common terminal is designated 0. Once the switcher, which is the problematic part of the converter, is modeled, the rest of the converter circuit is just a linear circuit and easily lends itself to modelling. To clarify the modeling procedure, an example of switched inductor Buck converter is presented as below.

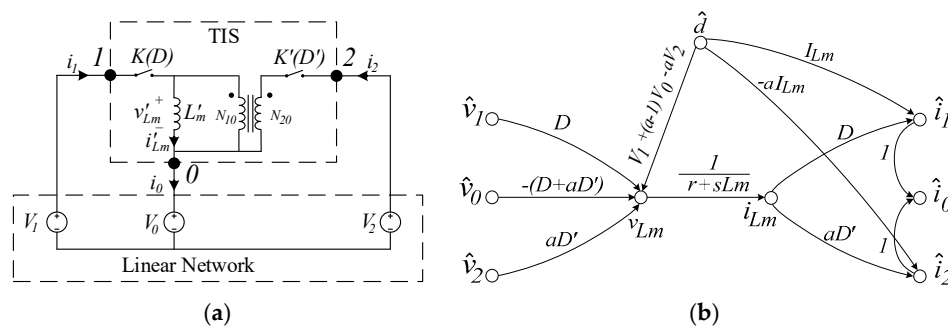


Figure 13. TIS block and its reference voltages and currents (a); Tapped Inductor Switcher (TIS)-SFG averaged small-signal model (b).

7.2. Example: TIS SFG Dynamic Models of TIBk and SIBk

As mentioned above, the SIBk converter in Figure 3 is equivalent to the TIBk converter in Figure 4 which has same frequency response and steady state performance, thus, the SIBk model is identical to the model of an ideal TIBk. The latter can be derived by the TIS-SFG method [22]. First, the switching part of the converter is symbolically substituted by the TIS block, complemented by the flow graph of the linear part of the converter as shown in Figure 14b. Here the output filter and load are modeled by a single equivalent branch (shown in blue). Then the TIS-SFG small signal model in Figure 13b is point-to-point substituted into Figure 14b. simplification of the graph yields the averaged small signal model of the TIBk converter as illustrated in Figure 14c. The ideal model in Figure 14c does not account for the capacitor's equivalent series resistance (ESR) as well as for parasitic resistances of the inductor and the switches.

Note that the capital letters in Figure 14c designate the steady-state values, whereas the hatted variables designate the small-signal variations of the respected quantities. For instance, the steady state duty cycle is labeled D and its small-signal variation by \hat{d} . As usual $D' = 1 - D$.

As shown above, with the parameters properly adjusted, the dynamic model of SIBk converter is identical to that of the TIBk converter. Hence, the small-signal averaged model of the SIBk converter can be derived by applying the equivalence conditions of Equations (5), (8), and (9) to Figure 14c to properly modify the equivalent inductance and the winding ratio. Note that the winding ratio, a in Figure 14 is defined as [22]:

$$a = \frac{N_1 + N_2}{N_2} = 1 + \frac{1}{n} \quad (16)$$

and $n = N_2/N_1$ is the turn ratio. Substitution of Equation (6) into Equation (16), results in $a = 2$. Substitution of Equations (8) and (9) into Figure 14c, this leads to the model in Figure 14d. Note that here, the effect of the capacitor's equivalent series resistance (ESR), r_C , is incorporated simply by

modifying the transfer function of the filter and load branch, whereas the combined effect of parasitic resistances of the switch, r_F , the diodes, r_{on} , and inductors, r_L , is modelled by a single inductor's equivalent series resistor, r . The derivation of the generalized equivalent series parasitic resistor, r , was presented in [22]. Here, r can be estimated as

$$r = r_L + \frac{1}{2}Dr_{on} + D'r_F \quad (17)$$

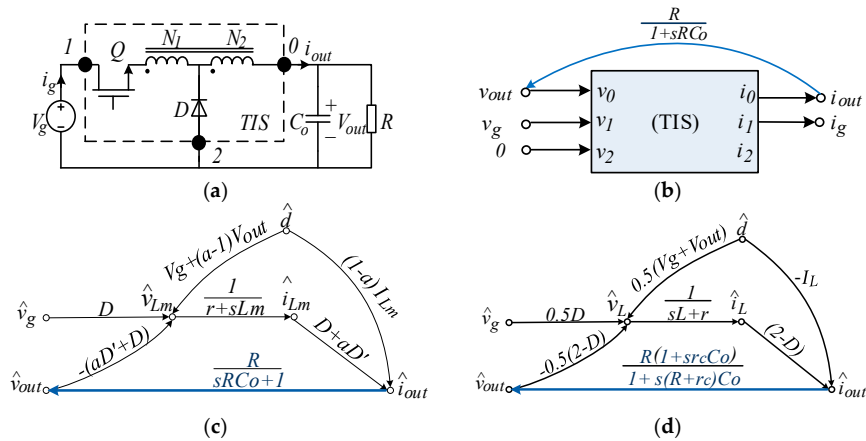


Figure 14. (a) Schematic diagram of the TIBk converter; (b) general TIS-SFG model of the ideal TIBk converter; (c) TIS-SFG averaged small-signal model of ideal TIBk converter; (d) the derived TIS-SFG average small-signal model of the non-ideal SIBk converter. The blue branch represents the capacitive filter and the load.

8. Experimental Verification

To experimentally verify the analysis above, a laboratory SIBk converter and its equivalent TIBk converter prototype were designed, built, and tested. The prototype of the SIBk converter had the following parameters: the inductors, $L_1 = 213.2 \mu\text{H}$, $L_2 = 213.2 \mu\text{H}$; switching frequency: $f_s = 46.92 \text{ KHz}$; input voltage: $V_{in} = 24 \text{ V}$; Output capacitor: $C_o = 47 \mu\text{F}$; load resistor: $R = 10 \text{ Ohm}$. At the duty cycle of $D = 0.5014$ the circuit was operated in CCM. The measured output dc voltage was 7.84 V and the measured efficiency was 96.01% .

The TIBk converter had the following parameters: the inductance of the primary side of the tapped inductor is $L_{N1} = 102.89 \mu\text{H}$, turns ratio of the tapped inductor: $n = 1$, the magnetizing inductance of the tapped inductor can be calculated as, $L_m = (1 + n^2)L_{N1} = 411.56 \mu\text{H}$; switching frequency is $f_s = 46.5 \text{ KHz}$; input voltage: $V_{in} = 24 \text{ V}$, output capacitor: $C_o = 47 \mu\text{F}$; load resistor: $R = 10 \text{ Ohm}$. At the duty cycle of $D = 0.5035$ the circuit was operated in CCM. The measured output dc voltage was 7.68 V and the measured efficiency was 93.72% .

The test bench of the prototype circuit is shown in Figure 15, while the experimental waveforms of SIBk and TIBk are shown in Figures 16 and 17. The input current, output current of the two circuits are compared in Figure 16a, while the voltage over MOSFET, v_{ds} , are shown in Figure 16b. The waveforms of the two converters are almost identical. Only a small difference is observed, except the higher voltage spike, v_{ds} , in the TIBk circuit.

The dynamic response of the SIBk circuit was also calculated and tested. The dynamic model of SIBk in Figure 14d requires the steady state solution data in order to calculate the gain of various branches of the model, which was derived the same as [6]

$$V_{out} = V_g \frac{D}{(2-D)}, \quad (18)$$

$$I_L = \frac{V_g}{R} \frac{D}{(2-D)^2}, \quad (19)$$

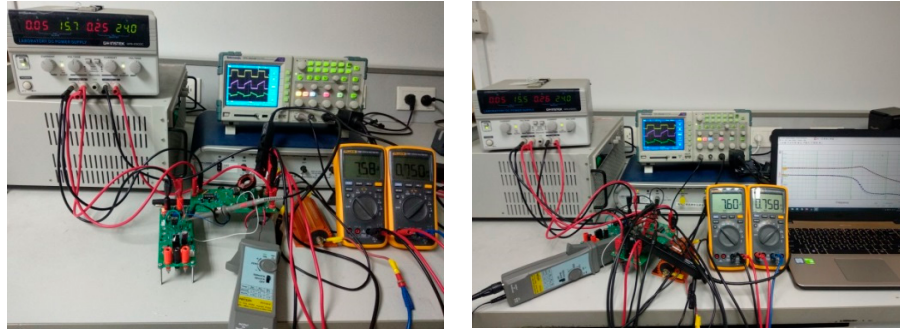
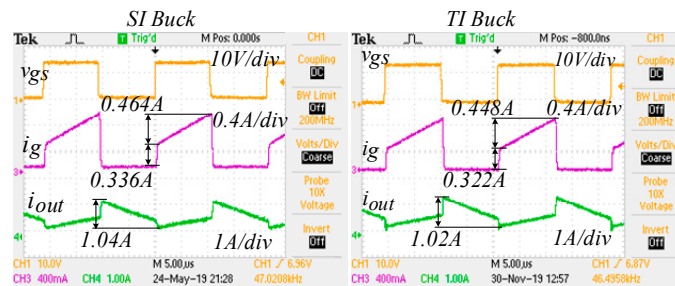
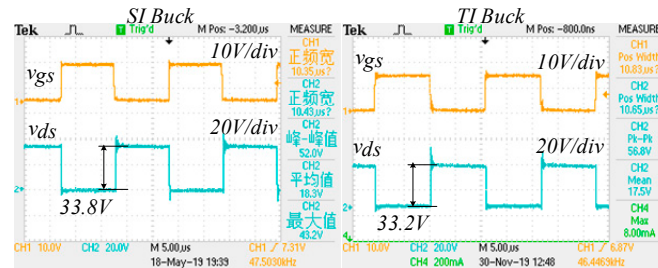


Figure 15. The test bench of the prototype circuit.



(a)



(b)

Figure 16. Comparison of experimental waveforms of SIBk vs. the equivalent TIBk converters in CCM. (a) the output current i_{out} ; the input terminal current i_g ; (b) the gating signal v_{gs} , Drain-to-Source voltage of MOSFET v_{ds} .

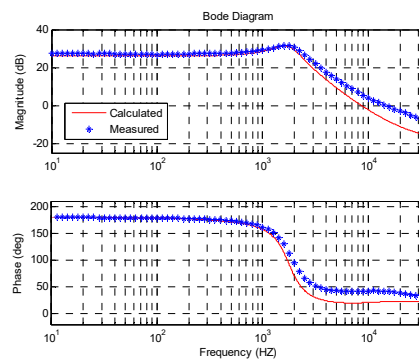


Figure 17. Comparison of the experimentally measured small signal duty-cycle to output voltage frequency response vs. the calculated non-ideal (Equation (20)) response of the SIBk converter.

The non-ideal small signal duty-cycle to output voltage transfer function was obtained from Figure 14d as

$$\frac{\hat{v}_{out}}{\hat{d}} = \frac{G(1 + \frac{s}{\omega_{z1}})(1 + \frac{s}{\omega_{z2}})}{1 + \frac{s}{Q\omega_0} + (\frac{s}{\omega_0})^2}, \quad (20)$$

where,

$$G = \frac{V_g}{(2-D)^2} \frac{[2R(2-D)^2 - Dr]}{[r + R(2-D)^2]}, \quad \omega_{z1} = \frac{[2R(2-D)^2 - Dr]}{2DL}, \quad \omega_{z2} = \frac{1}{r_c C}, \quad \omega_0 = \sqrt{\frac{R(2-D)^2 + r}{2LC_0(R+r_c)}}, \quad \text{and } Q = \frac{\sqrt{[r + R(2-D)^2]2LC_0(R+r_c)}}{[Rr_c C_0(2-D)^2 + C_0 r(R+r_c) + 2L]}.$$

The inductors' resistance was measured as $r_L = 0.08 \text{ Ohm}$; the switch on resistance of the MOSFET (30N06B), is $r_{on} = 0.025 \text{ Ohm}$; and the diodes' (MBR40250) forward resistance is predicted by the measured switch-on voltage drop and current which is $r_F = 1.12 \text{ Ohm}$. Plugging the aforementioned parameters into Equation (17) yields $r = 0.67 \text{ Ohm}$.

The dynamic response of the SIBk circuit was measured by Venable 8805 frequency response analyzer. The comparison of the calculated vs. experimentally measured responses is shown in Figure 17. The predicted response is well matched to the measurements and correctly predicts the gain peaking. Yet, some deviation can be seen at high frequency range due to uncertainties in the component values and the increase in the ac resistance of the inductors at high frequency.

9. Conclusions

The paper is concerned with the analogy existing in between the switched inductor converters and the tapped inductor converters. The equivalent counterparts were proposed and examined. The rules of equivalence were derived for several study cases: Switched Inductor modified Buck, Buck-Boost, Boost converters as well as Cuk, Sepic, and Zeta derived converters.

Practical implication of the proposed equivalence hypothesis is extending the TIS-SFG modelling approach [22], conceived for the TI converters, to include switched inductor converters as well. This paper illustrates the small signal modelling of the step-down SI cell to complete the step-up SI cell counterpart model demonstrated earlier [21]. As an example, SI Buck converter is analyzed theoretically and confirmed vs. simulated and experimental results.

The equivalence of TI and SI converters is somewhat limited in reality since the practical TI converters are prone to the problems of the leakage inductance. This, however, presents no hindrance to the suggested methodology of small-signal modeling the SI converters. As mentioned, SI converters have no leakage and, for this reason, the small-signal model of SI converter derived from the ideal (i.e., leakage-free) TI model attains accurate results in reality. Hence, taking advantage of the equivalence feature, and using the TIS model as a tool, can facilitate the small-signal analysis of SI converters.

Theoretical expectations were confirmed by an extensive cycle-by-cycle simulation study. The time-domain waveforms of the ideal switched inductor converters were compared and perfectly matched the waveforms of their equivalent ideal tapped-inductor counterparts. The equivalence holds in both continuous and discontinuous operating modes. Moreover, the performance of the Buck, Boost, and Buck-Boost equivalent converters in the frequency domain was also examined. The duty-cycle-to-output-frequency response of the switched inductor converters was simulated and compared to the response of their tapped inductor counterparts and, as expected, was found identical. Comparison of the experimental results for SIBk and TIBk converters was also reported. A good match was observed.

Author Contributions: Conceptualization, A.A. and J.Y.; Validation, K.L. and K.Z.; Writing-Original Draft Preparation, J.Y.; Writing-Review & Editing, A.A.; Project Administration, J.Y.; Funding Acquisition, J.Y.

Funding: This research was funded by the National Natural Science Foundation of China under Grant 51707096.

Conflicts of Interest: The authors declare no conflict of interest.

Appendix A

Extensive simulation study was launched to compare the SI topologies in Table 2 to their proposed TI equivalent counterparts. PSIM v 9.1.4 was used to run cycle-by-cycle time domain simulation of the candidate equivalent converters and their waveforms compared. The benchmark converters were operated in both the continuous and discontinuous modes. The simulation results are presented in Figures A1–A7. In all cases the simulated responses of both SI converters and their equivalent TI converters were found precisely identical. This supports the proposed notion of converter equivalence.

Furthermore, to verify the claim that the step-up SI cells in Figure 1a,b are identical, the time domain waveforms of an ideal SI Cuk in Table 2 (a) vs. SI Sepic in Table 2 (b) are compared in Figure A3. The time domain response of these two converters were found identical.

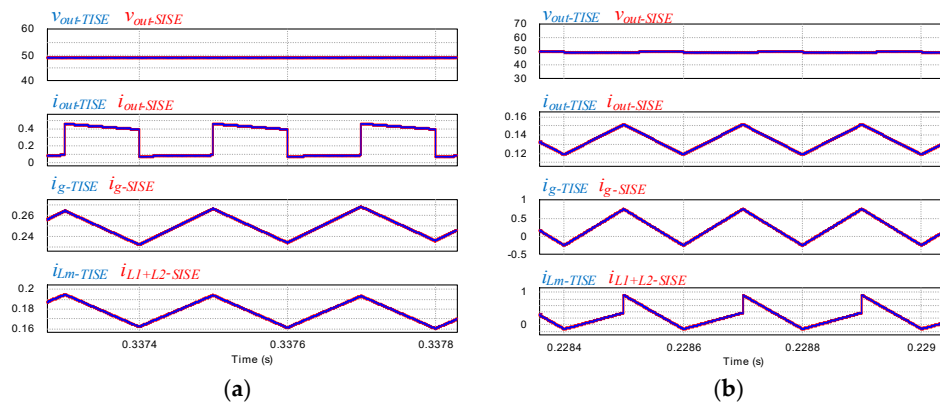


Figure A1. Comparison of time domain waveforms of an ideal SI Sepic (Step down) in Table 2 (b) vs. the equivalent TIS converters in Table 2 (e): (a) CCM; (b) DCM. Top trace: output voltage, V_{out} ; second trace: the output current, i_{out} ; third trace: the input terminal current, i_g ; bottom trace: the inductor current, i_L . (Parameters: $V_g = 100$ V, $D = 0.5$, $C = 150$ μ F, $C_o = 180$ μ F, $L_{in} = 300$ mH, $f_s = 50$ kHz and $R = 20$ Ohm. The inductors of the benchmark SI Sepic converter were $L_1 = L_2 = 300$ mH for CCM and 3 mH for DCM, whereas the tapped inductor of the equivalent TI Sepic converter: $n = 1$ and $L_m = 150$ mH for CCM and 1.5 mH for DCM.)

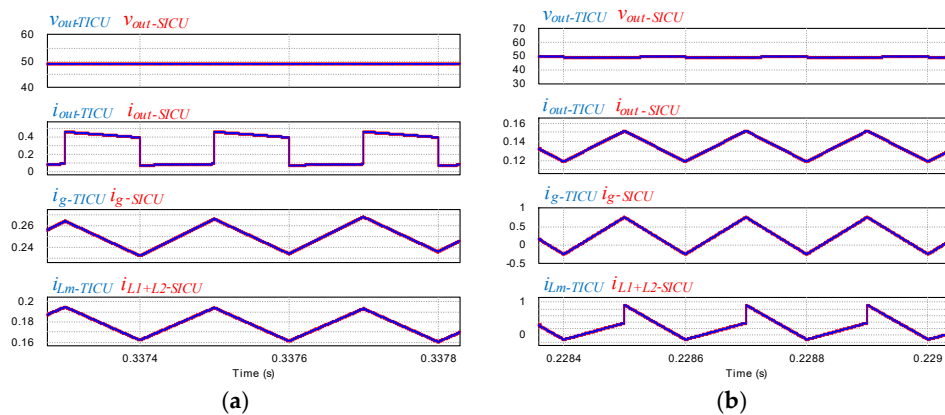


Figure A2. Comparison of time domain waveforms of an ideal SI Cuk (Step down) in Table 2 (a) vs. the equivalent TIS converters in Table 2 (d): (a) CCM; (b) DCM. Top trace: output voltage, V_{out} ; second trace: the output current, i_{out} ; third trace: the input terminal current, i_g ; bottom trace: the inductor current, i_L . (Parameters: $V_g = 100$ V, $D = 0.5$, $C = 150$ μ F, $C_o = 180$ μ F, $L_{in} = 300$ mH, $f_s = 50$ kHz and $R = 20$ Ohm. The inductors of the benchmark SI Cuk converter were $L_1 = L_2 = 300$ mH for CCM and 3 mH for DCM, whereas the tapped inductor of the equivalent TI Cuk converter: $n = 1$ and $L_m = 150$ mH for CCM and 1.5 mH for DCM.)

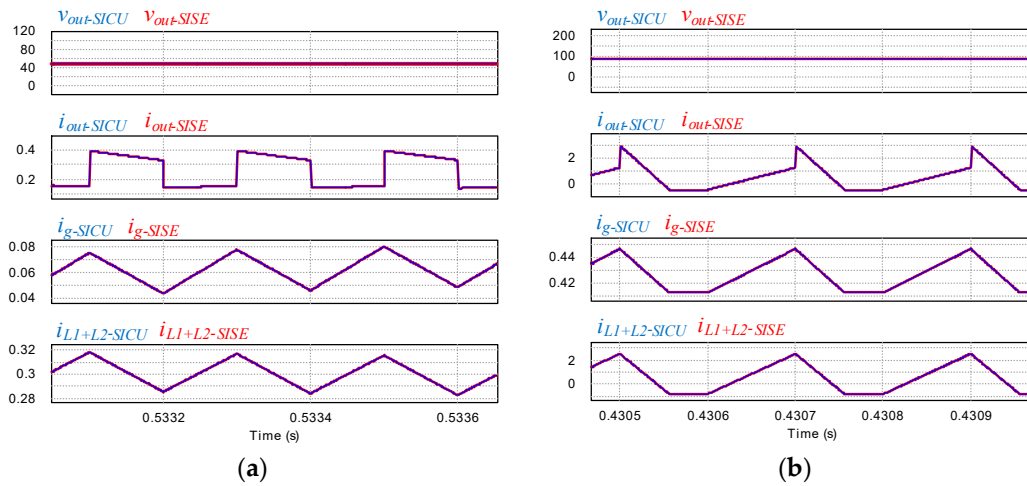


Figure A3. Comparison of time domain waveforms of an ideal SI Cuk (Step down) in Table 2 (a) vs. SI Sepic in Table 2 (b): (a) CCM; (b) DCM. Top trace: output voltage, V_{out} ; second trace: the output current, i_{out} ; third trace: the input terminal current, i_g ; bottom trace: the inductor current, i_L .

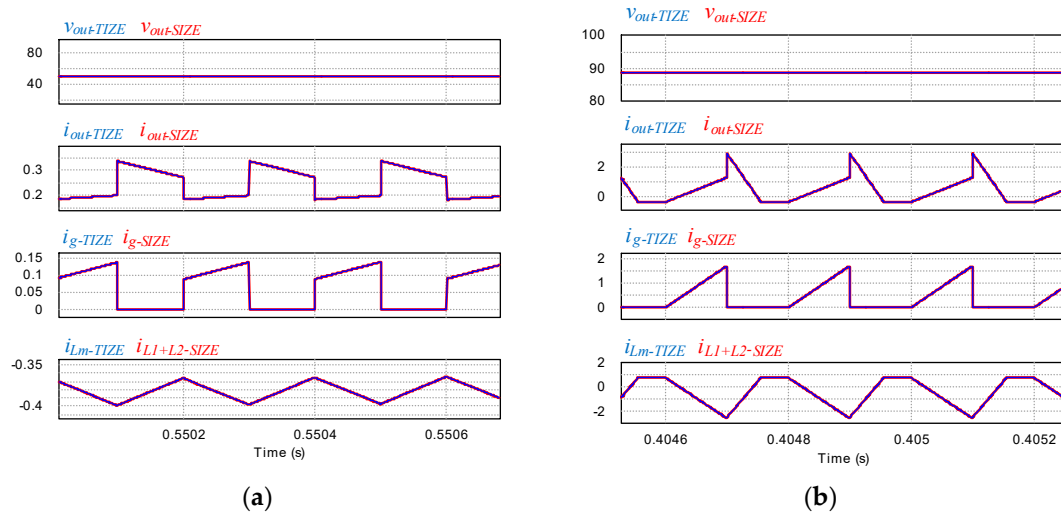


Figure A4. Comparison of time domain waveforms of an ideal SI Zeta (Step down) in Table 2 (c) vs. the equivalent TIS converters in Table 2 (f): (a) CCM; (b) DCM. Top trace: output voltage, V_{out} ; second trace: the output current, i_{out} ; third trace: the input terminal current, i_g ; bottom trace: the inductor current, i_L . (Parameters: $V_g = 100$ V, $D = 0.5$, $C = 150$ μ F, $C_o = 180$ μ F, $L_{in} = 300$ mH, $f_s = 50$ kHz and $R = 185$ Ohm. The inductors of the benchmark SI Zeta converter were $L_1 = L_2 = 300$ mH for CCM and 3 mH for DCM, whereas the tapped inductor of the equivalent TI Zeta converter: $n = 1$ and $L_m = 150$ mH for CCM and 1.5 mH for DCM.)

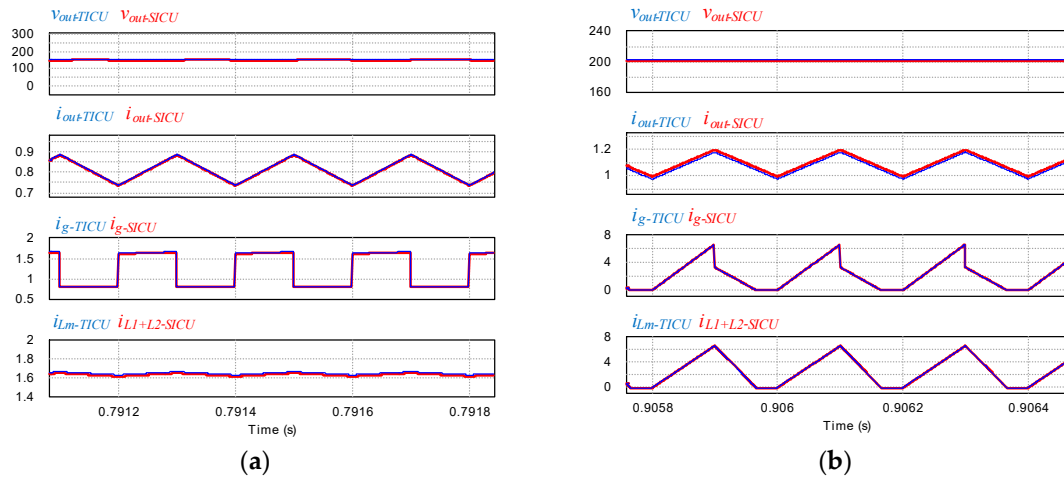


Figure A5. Comparison of time domain waveforms of an ideal SI Cuk (Step up) in Table 2 (g) vs. the equivalent TIS converters in Table 2 (j): (a) CCM; (b) DCM. Top trace: output voltage, V_{out} ; second trace: the output current, i_{out} ; third trace: the input terminal current, i_g ; bottom trace: the inductor current, i_L . (Parameters: $V_g = 100$ V, $D = 0.5$, $C = 100$ μ F, $C_o = 80$ μ F, $L_{out} = 100$ μ H, $f_s = 50$ kHz and $R = 185$ Ohm. The inductors of the benchmark SI Cuk converter were $L_1 = L_2 = 600$ mH for CCM and 3 mH for DCM, whereas the tapped inductor of the equivalent TI Cuk converter: $n = 1$ and $L_m = 300$ mH for CCM and 1.5 mH for DCM.)

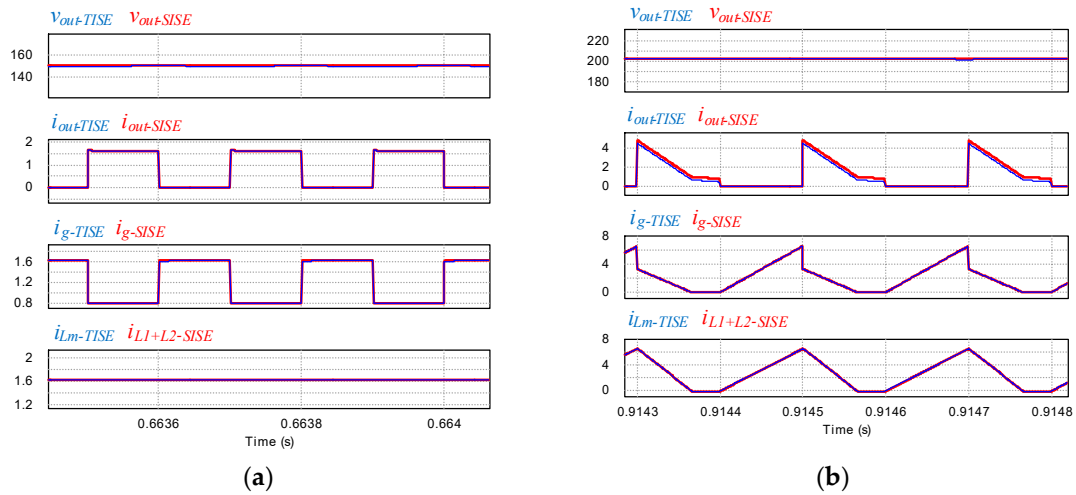


Figure A6. Comparison of time domain waveforms of an ideal SI Sepic (Step up) in Table 2 (h) vs. the equivalent TIS converters in Table 2 (k): (a) CCM; (b) DCM. Top trace: output voltage, V_{out} ; second trace: the output current, i_{out} ; third trace: the input terminal current, i_g ; bottom trace: the inductor current, i_L . (Parameters: $V_g = 100$ V, $D = 0.5$, $C = 150$ μ F, $C_o = 180$ μ F, $L_{in} = 300$ mH for CCM and 30 mH for DCM, $f_s = 50$ kHz and $R = 185$ Ohm. The inductors of the benchmark SI Sepic converter were $L_1 = L_2 = 1200$ mH for CCM and 3 mH for DCM, whereas the tapped inductor of the equivalent TI Sepic converter: $n = 1$ and $L_m = 600$ mH for CCM and 1.5 mH for DCM.)

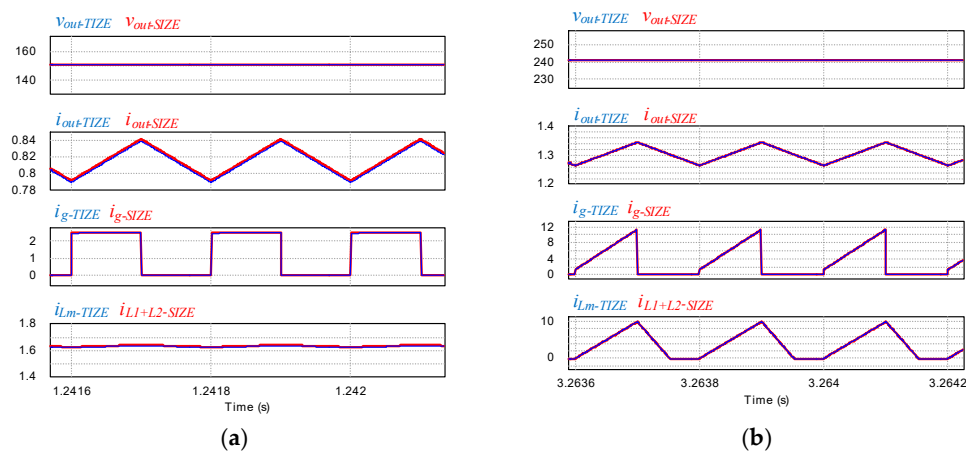


Figure A7. Comparison of time domain waveforms of an ideal SI Zeta (Step up) in Table 2 (i) vs. the equivalent TIS converters in Table 2 (l): (a) CCM; (b) DCM. Top trace: output voltage, V_{out} ; second trace: the output current, i_{out} ; third trace: the input terminal current, i_g ; bottom trace: the inductor current, i_L . (Parameters: $V_g = 100$ V, $D = 0.5$, $C = 150$ μ F, $C_o = 180$ μ F, $L_{out} = 300$ mH, $f_s = 50$ kHz and $R = 185$ Ohm. The inductors of the benchmark SI Zeta converter were $L_1 = L_2 = 1200$ mH for CCM and 2 mH for DCM, whereas the tapped inductor of the equivalent TI Zeta converter: $n = 1$ and $L_m = 600$ mH for CCM) and 1 mH for DCM.)

References

1. Liu, H.; Hu, H.; Wu, H. Overview of High-Step-Up Coupled-Inductor Boost converters. *IEEE J. Emerg. Sel. Top. Power Electron.* **2016**, *4*, 689–706. [\[CrossRef\]](#)
2. Surapaneni, R.K.; Das, P. A Z-Source-Derived Coupled-Inductor-Based High Voltage Gain Microinverter. *IEEE Trans. Ind. Electron.* **2018**, *65*, 5114–5124. [\[CrossRef\]](#)
3. Yao, J.; Abramovitz, A.; Smedley, K.M. Analysis and design of charge pump assisted high step-up tapped inductor Sepic converter with an Inductor-less regenerative snubber. *IEEE Trans. Power Electron.* **2015**, *30*, 5565–5580. [\[CrossRef\]](#)
4. Ye, Y.; Cheng, K.W.E.; Chen, S. A High Step-up PWM DC-DC Converter with Coupled-Inductor and Resonant Switched-Capacitor. *IEEE Trans. Power Electron.* **2017**, *32*, 7739–7749. [\[CrossRef\]](#)
5. Mohammadi, M.; Adib, E.; Yazdani, M.R. Family of Soft-Switching Single-Switch PWM Converters with Lossless Passive Snubber. *IEEE Trans. Ind. Electron.* **2015**, *62*, 3473–3481. [\[CrossRef\]](#)
6. Axelrod, B.; Berkovich, Y.; Ioinovici, A. Switched-Capacitor/Switched-Inductor Structures for Getting Transformerless Hybrid DC-DC PWM Converters. *IEEE Trans. Circuits Syst. I Reg. Pap.* **2008**, *55*, 687–696. [\[CrossRef\]](#)
7. Guilbert, D.; Collura, S.M.; Scipioni, A. DC/DC converter topologies for electrolyzers: State-of-the-art and remaining key issues. *Int. J. Hydrog. Energy* **2017**, *42*, 23966–23985. [\[CrossRef\]](#)
8. Li, S.; Li, Z.; Zheng, S.; Xie, W.; Zheng, Y.; Smedley, K. Multi-Resonance-Core-Based Dickson Resonant Switched-Capacitor Converters with Wide Regulation. *IEEE Trans. Power Electron.* **2020**, *35*, 1685–1698. [\[CrossRef\]](#)
9. Nguyen, M.K.; Le, T.V.; Park, S.J.; Lim, Y.C.; Yoo, J.Y. Class of high Boost inverters based on switched-inductor structure. *IET Power Electron.* **2015**, *8*, 750–759. [\[CrossRef\]](#)
10. Hu, Y.; Li, K.; Yin, Z.; Ioinovici, A. Switched-inductor-based non-isolated large conversion ratio, low components count DC-DC regulators. In Proceedings of the 2015 IEEE Energy Conversion Congress and Exposition (ECCE), Montreal, QC, Canada, 20–24 September 2015; pp. 1398–1405.
11. Cheng, K.W.E.; Ye, Y.M. Duality approach to the study of switched-inductor power converters and its higher-order variations. *IET Power Electron.* **2015**, *8*, 489–496. [\[CrossRef\]](#)
12. Zhu, X.; Zhang, B.; Li, Z.; Li, H.; Ran, L. Extended Switched-Boost DC-DC Converters Adopting Switched-Capacitor/Switched-Inductor Cells for High Step-up Conversion. *IEEE J. Emerg. Sel. Top. Power Electron.* **2017**, *5*, 1020–1030. [\[CrossRef\]](#)

13. Park, S.; Cha, G.; Jung, Y.; Won, C. Design and Application for PV Generation System Using a Soft-Switching Boost Converter With SARC. *IEEE Trans. Ind. Electron.* **2010**, *57*, 515–522. [[CrossRef](#)]
14. Yao, T.; Nan, C.; Ayyanar, R. A New Soft-Switching Topology for Switched Inductor High Gain Boost. *IEEE Trans. Ind. Appl.* **2018**, *54*, 2449–2458. [[CrossRef](#)]
15. Abdel-Rahim, O.; Orabi, M.; Abdelkarim, E.; Ahmed, M.; Youssef, M.Z. Switched inductor Boost converter for PV applications. In Proceedings of the 2012 Twenty-Seventh Annual IEEE Applied Power Electronics Conference and Exposition (APEC), Orlando, FL, USA, 5–9 February 2012; pp. 2100–2106.
16. Middlebrook, R.D.; Cuk, S. A general unified approach to modelling switching-converter power stages. In Proceedings of the IEEE Power Electronics Specialists Conference, Cleveland, OH, USA, 8–10 June 1976; pp. 18–34.
17. Ismeil, M.A.; Kouzou, A.; Kennel, R.; Ibrahim, A.A.; Orabi, M.; Ahmed, M.E. Modeling of non-ideal improved Switched Inductor (SL) Z-source inverter. In Proceedings of the International Aegean Conference on Electrical Machines and Power Electronics and Electromotion, Istanbul, Turkey, 8–10 September 2011; pp. 472–477.
18. Wang, F.; Li, J. Improved small signal modeling and dynamic analysis of high step-up converter with charged pump and Boost converter. In Proceedings of the 2016 IEEE 11th Conference on Industrial Electronics and Applications (ICIEA), Hefei, China, 5–7 June 2016; pp. 495–499.
19. Hwu, K.I.; Yau, Y.T. High Step-Up Converter Based on Charge Pump and Boost Converter. *IEEE Trans. Power Electron.* **2012**, *27*, 2484–2494. [[CrossRef](#)]
20. Zhang, Y.; Dong, Z.; Liu, J.; Liu, Y. Unified model of high step-up DC-DC converter with multi-cell diode-capacitor/inductor network. In Proceedings of the 2016 IEEE Energy Conversion Congress and Exposition (ECCE), Milwaukee, WI, USA, 18–22 September 2016; pp. 1–8.
21. Yao, J.; Zheng, K.; Abramovitz, A. Small Signal Model of Switched Inductor Boost Converter. *IEEE Trans. Power Electron.* **2019**, *34*, 4036–4040. [[CrossRef](#)]
22. Abramovitz, A.; Yao, J.; Smedley, K. Unified Modeling of PWM Converters with Regular or Tapped Inductors Using TIS-SFG Approach. *IEEE Trans. Power Electron.* **2016**, *31*, 1702–1716. [[CrossRef](#)]
23. Luo, F.L.; Ye, H. Super-lift Boost converters. *IET Power Electron.* **2014**, *7*, 1655–1664. [[CrossRef](#)]
24. Chen, Y.; Tsai, M.; Liang, R. DC–DC converter with high voltage gain and reduced switch stress. *IET Power Electron.* **2014**, *7*, 2564–2571. [[CrossRef](#)]
25. Wu, T. Decoding and Synthesizing Transformerless PWM Converters. *IEEE Trans. Power Electron.* **2016**, *31*, 6293–6304. [[CrossRef](#)]
26. Yao, J.; Abramovitz, A. Abramovitz, Fast SFG Modeling of Integrated Converters. *IEEE J. Emerg. Sel. Top. Power Electron.* **2017**, *5*, 1008–1019. [[CrossRef](#)]

